

Phase Diagram and Physical Properties of H₂O at High Pressures and Temperatures: Applications to Planetary Interiors

Jung-Fu Lin, Eric Schwegler, and Choong-Shik Yoo

Lawrence Livermore National Laboratory, 7000 East Avenue, Livermore, CA 94550

Here we discuss the phase diagram and physical properties of H₂O under pressure-temperature conditions relevant to planetary interiors. Recent studies show that the melting curve of H₂O increases rapidly above a recently discovered triple point at approximately 35 to 47 GPa and 1000 K, indicating a large increase in $\Delta V/\Delta S$ (volume versus entropy change) and associated changes in the physical properties of H₂O at high pressures and temperatures. Existence of the triple point is thought to be associated with the formation of a superionic phase, dynamically-disordered ice VII, or extension of the ice VII-ice X phase boundary; although the precise pressure and temperature of the triple point, curvature of the melting line, and nature of the solid-solid transition below the triple point all remain to be further explored. The steep increase in the melting curve of H₂O at high pressures and temperatures has important implications on our understanding of planetary interiors. Depending on its curvature, the melting line of H₂O may intersect the isentropes of Neptune and Uranus as well as the geotherm of Earth's lower mantle. Furthermore, if the triple point is due to the occurrence of the theoretically predicted superionic phase, besides leading to significant ionic conductivity, fast proton diffusion would cause enhanced chemical reactivity and formation of complex compounds in these planets. For example, reaction of H₂O with iron and other metals to form metal hydrides such as FeH_x could provide a mechanism for incorporation of hydrogen as a light element into Earth's core. The equation of state of water is also presented as it pertains to the properties of hydrous fluid and melt phases in the mantle.

INTRODUCTION

Due to a triple point that occurs near the Earth's mean surface temperature and pressure, H₂O is present in three different forms within the biosphere; water, vapor, and solid ice-Ih. H₂O is also believed to be a major component of the intermediate ice layers in the interiors of Uranus and Neptune [Nellis *et al.*, 1988; Hubbard *et al.*, 1991],

and water vapor plumes have been detected near the south polar regions of Saturn's icy moon, Enceladus [Hansen *et al.*, 2006]. Water is also a major component of fluid and melt phases forming in the Earth's mantle on dehydration. Based upon the bulk water content of ordinary chondritic meteorites, two-thirds of Earth's original H₂O may have either been lost to space or is present in the interior as trace quantities of (OH)⁻ in nominally anhydrous mantle minerals [e.g. Smyth, 1987; Bell and Rossman, 1992; Williams and Hemley, 2001; see Smyth and Jacobsen, 2006, *this volume for a review*]. Deep reservoirs of H₂O may also present in dense magnesium silicates [e.g. Angel *et al.*, 2001; also see

Komabayashi *et al.*, (2006) of this volume] or even as ice-VII in cold subducting slabs [Bina and Navrotsky, 2000]. Therefore, the physical and chemical properties of H₂O at high pressures and temperatures (*P-T*) play an important role in planetary science. The behavior and phase diagram of H₂O at high *P-T* are also of fundamental interest in physics, chemistry, and biological sciences because the flexibility of hydrogen bonding gives rise to a myriad of crystalline, amorphous, and liquid phases with unique physical and chemical properties [Petrenko and Whitworth, 1999].

Shock-wave experiments have served as the main tool to characterize liquid water under high *P-T*. The results have been used to derive and to constrain a variety of equation of state (EOS) models [Holmes *et al.*, 1985; Nellis *et al.*, 1988]. Shock wave studies have also been used to determine additional properties of water at high pressure such as Raman spectra [Holmes *et al.*, 1985] and electrical conductivity [David *et al.*, 1960; Hamann *et al.*, 1969; Holzapfel, 1969; Mitchell *et al.*, 1982; Chau *et al.*, 2001; Celliers *et al.*, 2004]. These experiments suggest that high *P-T* conditions generate highly mobile charge carriers through molecular dissociation leading to an increase in ionic conductivity [David *et al.*, 1960; Hamann *et al.*, 1969; Holzapfel, 1969; Mitchell *et al.*, 1982; Chau *et al.*, 2001] and eventually to the onset of electronic conduction in liquid water [Celliers *et al.*, 2004].

In addition to shockwave and theoretical studies, static measurements of the melting curve, phase behavior, and physical properties of H₂O have recently been performed under *P-T* conditions that are relevant to the interior of planets, such as Earth. These studies have found strong evidence for a rapid increase in the melting temperature of H₂O above 35 to 47 GPa. Here we discuss recent developments in high-pressure experimental and theoretical studies on the behavior and physical properties of H₂O in terms of possible implications for planetary interiors.

HIGH *P-T* PHASES OF H₂O

Our current understanding of the phase diagram of H₂O is summarized in Figure 1. In the following, we will focus primarily on the high *PT* regions that are most relevant to planetary interiors (the liquid and solid phases above 2 GPa and 300 K). As illustrated in Figure 2a, Ice VII is a molecular crystal consisting of oxygen atoms arranged on a body-centered cubic (*bcc*) lattice and hydrogen atoms arranged in random (disordered) positions that satisfy the ice rules. The overall structure is often described as two interpenetrating hydrogen bond networks of cubic ice disconnected in the sense that they do not share any hydrogen bonds in common. In addition, there is experimental evidence that in the range of 2.2 to 25 GPa, ice VII exhibits spatially modulated

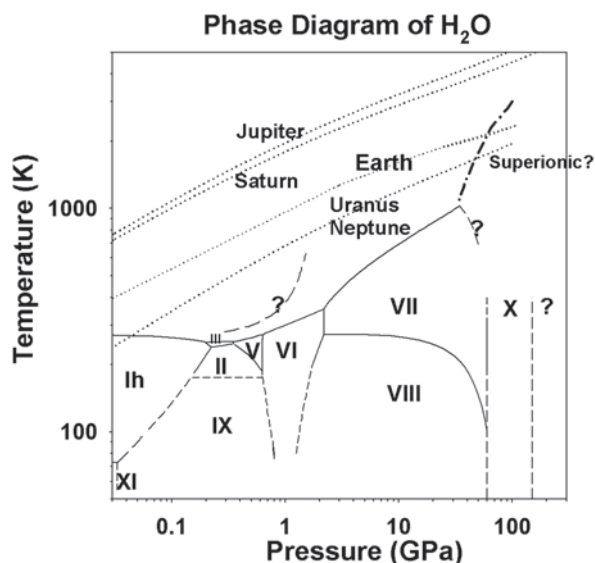


Figure 1. High *P-T* phase diagram of H₂O. The Roman numerals are various forms of solid ices, whereas ice Ih represents ice in the hexagonal crystal structure. Black solid line, experimentally determined phase boundaries [after Petrenko and Whitworth, 1999; Lin *et al.*, 2005]; dash line: schematic phase boundaries; dotted lines: isentropes of Jupiter, Saturn, Uranus, and Neptune [de Pater and Lissauer, 2001], respectively, and geotherm of the Earth [Brown and Shankland, 1981]. The dash line in the liquid region represents a proposed liquid-liquid transition by Kawamoto *et al.* [2004]. At pressures near 150 GPa additional structural phase transitions have been proposed based on both theory [Demontis *et al.*, 1988; Benoit *et al.*, 1996] and experiment [Loubeyre *et al.*, 1999]. Depending on the curvature of the extrapolated melting curve above 35 GPa (dash-dotted line), the melting curve may intersect proposed isentropes of Neptune and Uranus at ~50 GPa and geotherm at ~60 GPa [Lin *et al.*, 2005].

(incommensurate) phases; a modulation in the periodicity of the structure [Loubeyre *et al.*, 1999].

All of the ice phases observed below 60 GPa have structures that closely follow Pauling's ice rules [Pauling, 1935]: 1) molecular crystals composed of water molecules with "gas-phase" like geometries, 2) each water molecule is oriented so that it participates in four hydrogen bonds with neighboring water molecules in tetrahedral coordination, and 3) at most one hydrogen atom is located between any two neighboring oxygen atoms. However, at higher pressures the ice rules are no longer satisfied as symmetrization of the hydrogen bond leads to protons residing midway between adjacent oxygen atoms, resulting in stable forms of ice that are non-molecular [Holzapfel, 1972; Polian *et al.*, 1984; Benoit *et al.*, 1996; Aoki *et al.*, 1996; Goncharov *et al.*, 1996,

1999; Loubeyre *et al.*, 1999]. As illustrated in Figure 2b, with increasing pressure, nearest neighbor oxygen-oxygen distances in ice VII decrease, and eventually in the pressure range of 40 to 60 GPa the hydrogen atoms are located at the midway point between neighboring oxygen atoms leading to a transition from a molecular to an atomic crystal called ice X. At even higher pressures, near 150 GPa, additional structural phase transitions have been proposed based on both theory [Demontis *et al.*, 1988; Benoit *et al.*, 1996] and experiment [Loubeyre *et al.*, 1999] where the *bcc* oxygen sublattice in ice X undergoes a transformation to an anti-fluorite or a hexagonal-close packed (*hcp*) structure.

In addition to the intriguing high *P*, low *T* behavior of ice, *ab initio* simulations indicate that the high *P-T* behavior of H₂O may hold surprises as well. For instance, it has been predicted that many of the high *P-T* phases of ice have regions characterized by fast protonic diffusion with stable oxygen sublattices, which could lead to significant increases in ionic conductivity while still in the solid phase [Demontis *et al.*, 1988; Benoit *et al.*, 1996; Cavazzoni *et al.*, 1999; Goldman *et al.*, 2005]. These high *P-T* domains of fast proton diffusion in ice are often referred to as a superionic phase [Cavazzoni *et al.*, 1999; Goldman *et al.*, 2005].

The liquid phase of H₂O also undergoes significant changes with increasing *P-T*. In particular, the local structure of liquid H₂O changes from the open four-fold hydrogen bonded structure at ambient *P-T* conditions to a nearest-neighbor coordination shell of up to 13 at pressures of 10 GPa (Figure 2c) [Schwegler *et al.*, 2000; Strässle *et al.*, 2006]. This change from low to high density H₂O appears gradually based on neutron diffraction studies up to 400 MPa [Soper *et al.*, 2000]. However, there is also indirect evidence from

Raman spectroscopy that the transition is abrupt and possibly first-order [Kawamoto *et al.*, 2004]. It is perhaps surprising to note that below 15 GPa and at temperatures near the melting curve, the large increase in coordination number from four-fold bonded to higher nearest-neighbor coordination is not accompanied by a corresponding decrease in the average nearest neighbor oxygen-oxygen distance or an appreciable change in the number of hydrogen bonds [Schwegler *et al.*, 2000; Strässle *et al.*, 2006]. Although this process is typically referred to as a simple collapse of the second coordination shell down on the first [Schwegler *et al.*, 2000; Soper *et al.*, 2000], one could speculate that the collapse occurs primarily between H₂O molecules that are not connected via “hydrogen bond wires”, and results in a set of interpenetrating hydrogen bond networks in the high-density liquid that closely resembles structures of the ice phases (*e.g.* ice VII) found at corresponding pressures (Figure 2).

Shock wave studies have shown that the conductivity of liquid water increases rapidly along the primary Hugoniot (the locus of states reached by passage of a shock wave through a material initially at ambient *P-T* conditions) above 10 GPa and eventually levels off to values typical of molten ionic salt above 20 GPa [Nellis *et al.*, 1988]. The increased conductivity of liquid H₂O at high *P-T* is commonly interpreted as being caused by a rapid increase in the fraction of dissociated H₂O molecules in the liquid [Holzapfel, 1969]. As illustrated in Figure 2c, a similar onset of molecular dissociation in water is found in *ab initio* MD simulations [Schwegler *et al.*, 2001] and estimates of the ionic conductivity along the planetary isentrope of Uranus agree well between simulation [Cavazzoni *et al.*, 1999] and reverberating shock measurements [Chau *et al.*, 2001].

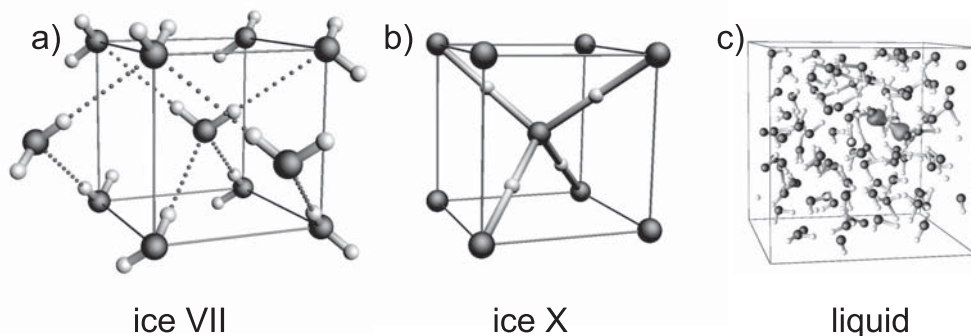


Figure 2. Schematic representations of ice VII (a), ice X (b), and a snapshot from an *ab initio* MD simulation of liquid water at 27 GPa and 1400 K (c) [Schwegler *et al.*, 2001]. The large black spheres represent oxygen atoms, the small white spheres are hydrogen atoms, and the black dashed/dotted lines in Fig. 2a are hydrogen bonds. The isosurfaces in Fig. 2c are the orbitals involved in a typical dissociation event in the liquid as a proton is shuttled between neighboring oxygen atoms.

EXPERIMENTAL AND THEORETICAL METHODS
AT HIGH *P-T*

A variety of techniques have been used to study the behavior of H₂O under extreme conditions. Here we focus on static and theoretical methods capable of reaching *P-T* conditions relevant to planetary interiors. In particular, externally-heated diamond anvil cells (EHDAC) and laser-heated diamond anvil cells (LHDAC) are two common high-pressure techniques used to reach to static high *P-T* conditions [Bassett *et al.*, 1993; Fei *et al.*, 1993; Lin *et al.*, 2004a]. Because commonly used pressure calibrants such as samarium-doped yttrium-aluminum-garnet (YAG) and ruby have a tendency to dissolve in water above 600 K (Dachi *et al.*, 2002), secondary holes near the sample chamber have been used to hold the pressure calibrant in optical spectroscopic studies [Lin *et al.*, 2004a]. In order to avoid reaction between H₂O and metal-based gasket materials, various other metal gaskets and gasket inserts, such as Re, Au, Ir, W, and Pt, have been tested and shown to successfully confine H₂O at high *P-T* [Lin *et al.*, 2005]. Inert pressure calibrants such as Au or Ta has also been used in thermal EOS studies with X-ray diffraction [Lin *et al.*, 2005]. The EHDAC apparatus can be readily interfaced with a variety of experimental probes, such as *in situ* Raman spectroscopy, X-ray diffraction, and/or visual observations for investigating the phase diagram of H₂O.

LHDACs have also proven to be a useful tool for studying H₂O at *in-situ* high *P-T* conditions. Because H₂O is transparent to the 1 μm infrared laser often used in these experiments, metal foils (Pt, Pt-Ir alloys, Ir, Re, or W) are used as a laser absorber, both with and without a small hole of 10–20 μm in diameter in the center of the foil [Schwager *et al.*, 2004; Goncharov *et al.*, 2005; Lin *et al.*, 2004b]. The temperature of the laser-heated sample can be determined from either the surface temperature of the foil [Schwager *et al.*, 2004] or from the intensity ratios of the Stokes-to-anti-Stokes Raman peaks [Goncharov *et al.*, 2005]. In these experiments, chemical reactions with Fe, Re, Pt, and W foils to form metal hydrides have been observed at high temperature [Schwager *et al.*, 2004; Lin *et al.*, 2005; Ohtani *et al.*, 2005], while Ir foils apparently react with H₂O only if the system is heated to several hundred degrees above the melting curve [Schwager *et al.*, 2004], and Pt-Ir (20% Ir) foils do not show any evidence of reactions with H₂O up to temperatures of 1500 K [Goncharov *et al.*, 2005]. Visual observation of changes in the laser-speckle pattern (Schwager *et al.*, 2004) or *in situ* Raman spectroscopy (Lin *et al.*, 2004b; Goncharov *et al.*, 2005) have recently been employed as criteria for identifying melting and structural phase transitions.

In addition to the recent developments in DAC technologies, first-principles theoretical approaches have proven to be a useful tool for investigating the high *P-T* properties of H₂O. Ever since the first classical molecular dynamics (MD) simulation of liquid H₂O [Rahman *et al.*, 1971], a great deal of effort has gone into the development of improved models. In fact, for modest *P-T* conditions, a variety of different classical potentials are known to accurately reproduce the properties of both the liquid and solid phases of H₂O [Mahoney *et al.*, 2000; Sanz *et al.*, 2004]. However, as one considers the extreme conditions that are relevant to planetary interiors, many of these simple empirical models are known to break down. This general failure is partly due to the overall lack of reliable experimental data to fit the potentials to, but more importantly, as higher *P-T* are considered, molecular dissociation begins to play a dominant role. For instance, at pressures above 15 GPa, the Hugoniot of water obtained from commonly used empirical potentials deviate significantly from experiment due to the empirical potentials' inability to describe molecular dissociation effects. It is in these regimes of high *P-T* where first-principles based methods can be used to go beyond the limitations of a typical classical model. In addition to providing enough predictive power to reliably investigate regions of phase space where there is little or no existing experimental data, first-principles methods are appropriate for investigating extreme *P-T* conditions, since bond making and breaking processes are taken into account in a quantitative fashion.

There are several notable exceptions to the general failure of empirical models (such as theoretical models with classical potentials) to describe H₂O under extreme conditions. For instance, a rather simple model based on Morse potentials was first used to successfully argue that hydrogen bond symmetrization should occur in ice VII as it is compressed, and eventually result in a transition to ice X [Holzapfel, 1972]. Subsequent calculations with increasingly sophisticated levels of theory such as *ab initio* MD and path integral sampling were used to further characterize the transition to ice X in much greater detail [Bernasconi *et al.*, 1998; Benoit *et al.*, 1998] and to propose additional structural phase transitions at higher pressures [Demontis *et al.*, 1988; Benoit *et al.*, 1996].

THE MELTING CURVES OF H₂O

Precise determination of the melting curve of H₂O is essential for modeling planetary interiors, understanding how numerous chemical reactions may affect the stability field of mineral assemblages at extreme conditions, and verifying theoretical predictions. Recently, conflicting reports on the melting curve of H₂O below ~30 GPa have been resolved using angle-dispersive synchrotron X-ray

diffraction, Raman spectroscopy, and visual observation as melting criteria [Lin *et al.*, 2004a; 2005] (Figures 3, 4 and Plate 1). The disappearance of diffraction peaks from the oxygen lattice of solid H₂O phases in an EHDAC has been used as an indication of melting in previous studies [Fei *et al.*, 1993; Dubrovinskaia and Dubrovinsky, 2003a,b; Frank *et al.*, 2004]. However, recrystallization of ice VII in different orientations at *P-T* conditions close to the melting line makes it difficult to identify the onset of the melting in such experiments [Datchi *et al.*, 2000; Lin *et al.*, 2004a]. Use of the very intense synchrotron X-ray source now makes it possible to detect diffuse X-ray scattering characteristic of water, providing a very reliable melting criterion (Figure 3). Future advances in modeling diffuse X-ray scattering patterns will further provide knowledge of the local structure of water at high *P-T*.

A change of Raman-active OH-stretching bands and the appearance of the translational modes (specific modes of

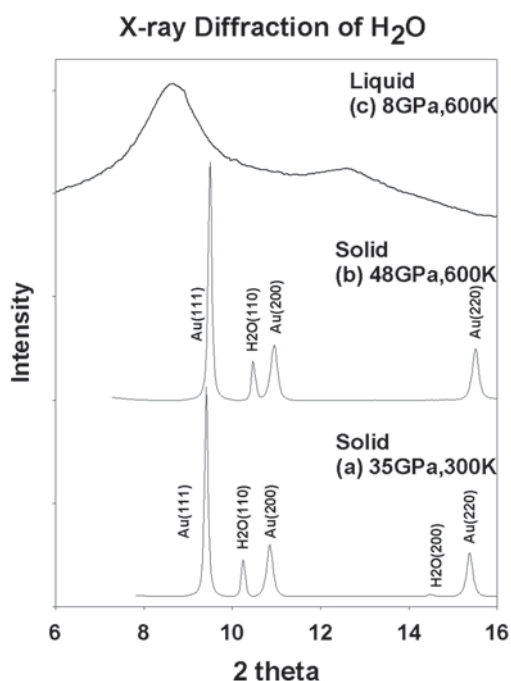


Figure 3. Angle-dispersive X-ray diffraction and diffuse scattering patterns of the solid (a,b) and liquid (c) H₂O at high *P-T*. A monochromatic beam (wavelength = 0.4157 Å) was used as the X-ray source and the diffracted X-rays were collected by a CCD (MARCCD). The diffraction patterns a and b showed diffraction peaks of the oxygen atoms in a bcc sublattice, indicating the existence of the solid ice phase. The observation of the diffuse scatterings (pattern c) showed clearly the occurrence of the liquid water under high *P-T*.

Raman Spectra of H₂O

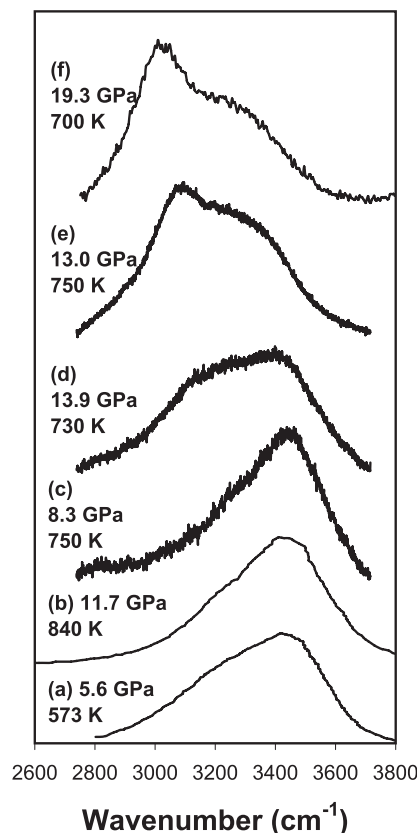


Figure 4. Representative Raman spectra in liquid and solid H₂O in shock wave (pattern a) [Holmes *et al.*, 1985] and static DAC (pattern b: Kawamoto *et al.*, 2004; patterns c,d,e,f: Lin *et al.*, 2004a; 2005) studies. a,b,c,d; liquid water; e,f: solid ice. The OH-stretching modes change significantly across melting; the low-frequency A_{1g} mode is the dominant band in ice VII while the high frequency mode dominates in liquid water. The change of the Raman-active OH-stretching bands can be used to detect melting [Lin *et al.*, 2004a; 2005].

the lattice vibrations) have also been used to reliably detect melting in ice VII (Figure 4) [Lin *et al.*, 2004a; Lin *et al.*, 2005]; the low-frequency A_{1g} mode is the dominant band in ice VII while the high frequency mode dominates in liquid water. The observed OH-stretching bands of liquid water at static high pressures are very similar to those obtained in shock-wave Raman measurements reaching to 26 GPa and 1700 K [Holmes *et al.*, 1985]. The intensity increase in the high frequency band obtained in the shock-wave experiments has been interpreted as an indication of an increase in monomeric water molecule concentration due to the

breaking of intermolecular hydrogen bonding [Holmes *et al.*, 1985]. In both static and shock wave Raman spectra measurements there is a lack of broad band centered at 2900 to 3000 cm⁻¹ that is characteristic of the hydronium ion (H₃O⁺) at low pressures [Holmes *et al.*, 1985; Kawamoto *et al.*, 2004; Lin *et al.*, 2004a; 2005]. This has led to the suggestion that the dissociation of water under high pressure conditions results in the formation of free H⁺ and OH⁻ ions, which in turn are responsible for the observed conductivity increase in water for pressures between 3 to 30 GPa [Holmes *et al.*, 1985; Chau *et al.*, 2001]. However, a series of *ab initio* MD simulations at similar thermodynamic conditions found evidence that the dissociation of water still occurs through a bimolecular process similar to what is found at ambient conditions, leading to the formation of short-lived OH⁻ and H₃O⁺ ions [Schwegler *et al.*, 2000; 2001]. For pressures above ~25 GPa, the OH-stretching modes begin to overlap with the second order Raman signal from the diamond anvils, making it difficult to use these modes to detect melting. Nevertheless, subtraction of the second-order Raman scattering of the diamond anvils from the Raman spectrum taken from a LHDAC has been used to measure the phase diagram of H₂O up to 56 GPa and 1500 K [Goncharov *et al.*, 2005].

Plate 1 shows a comparison of recent experimental and theoretical melting lines [Cavazzoni *et al.*, 1999; Dubrovinskaia *et al.*, 2003a,b; Frank *et al.*, 2004; Lin *et al.*, 2004a; Schwager *et al.*, 2004; Goldman *et al.*, 2005; Goncharov *et al.*, 2005; Lin *et al.*, 2005]. Although significant discrepancies occur in these reported melting curves, these studies, in general, point to a discontinuous increase along the melting line approximately between 35 GPa to 47 GPa. MD simulations from 30 to 300 GPa first indicated a discontinuous increase in the melting curve at high *P-T* relative to the extrapolated experimental melting curve of ice VII from lower *P-T* conditions [Cavazzoni *et al.*, 1999]. According to these and subsequent MD simulations, the change in slope is likely due to the appearance of a superionic phase below the melting curve [Cavazzoni *et al.*, 1999; Goncharov *et al.*, 2005; Goldman *et al.*, 2005]. On the experimental side, visual observations of the laser-speckle pattern in a LHDAC first reported a distinct change in melting slope at 43 GPa and 1600 K, and it was speculated that this change was due to a first-order transformation from ice VII to ice X [Schwager *et al.*, 2004]. *In situ* Raman spectroscopy in a LHDAC confirmed the discontinuous melting curve and indicated the presence of a triple point at about 47 GPa and 1000 K [Goncharov *et al.*, 2005], which is accompanied by a substantial decrease in the intensity of the O-H stretch band in the Raman spectra. Similar trends in the power spectra obtained in *ab initio* MD simulations

indicate that the observed change in the melting curve may be due to the occurrence of a superionic phase at high pressure [Goncharov *et al.*, 2005]. EHDAC experiments with *in-situ* X-ray diffraction, Raman spectroscopy, and reliable *P-T* determinations also showed a discontinuous change in the melting curve at approximately 35 GPa and 1040 K, although the melting temperature of H₂O above 40 GPa is beyond the temperature capability of the EHDAC, leading to a large uncertainty in the curvature of the extrapolated melting curve [Lin *et al.*, 2005]. Inconsistencies between reported melting lines from various experimental techniques highlight the importance of reliable melting criteria and precise *P-T* determinations, as well as the need for expanded high *P-T* capabilities and improved techniques for detecting subtle changes in oxygen-hydrogen bonding in future experimental studies of these unresolved regions of the high *P-T* phase diagram of H₂O.

There are also significant differences between recent theoretical studies of the melting curve of H₂O. For instance, *ab initio* MD calculations have predicted that at 2000 K, H₂O will melt at pressures ranging from 30 GPa [Cavazzoni *et al.*, 1999], to 65 GPa [Goncharov *et al.*, 2005], to 75 GPa [Goldman *et al.*, 2005]. The large discrepancy in the calculated melting pressures at 2000 K is somewhat surprising given the nearly identical levels of theory and simulation protocols used. In addition to issues related to finite size effects and simulation timescales, it is possible that a large fraction of this discrepancy comes from the specific computational approaches used to determine the phase boundary. In all of the previous investigations with *ab initio* MD, the simulations have started with a single phase (either the liquid or the solid) and have proceeded with a “heat-until-it-melts” or a “squeeze-until-it-freezes” strategy for locating the transition between the liquid and the solid phase. The primary objection to these types of approaches is that the observed phase transition does not directly correspond to the melting temperature (or pressure), but instead to conditions of thermal metastability, which for small system sizes and short simulation timescales can be significantly different from the equilibrium melting point. The two main approaches for reliably computing a material’s melting temperature is to use either a free-energy based method where the equivalence of the Gibbs free energy of the solid and the liquid is computed [Alfe, *et al.*, 2003], or a two-phase approach where coexistence between the solid and the liquid is directly simulated [Ogitsu *et al.*, 2003]. To date, neither of these computational techniques has been applied within an *ab initio* MD context to examine H₂O, and as such, the accurate computation of the high-pressure melting curve remains an open challenge to theorists.

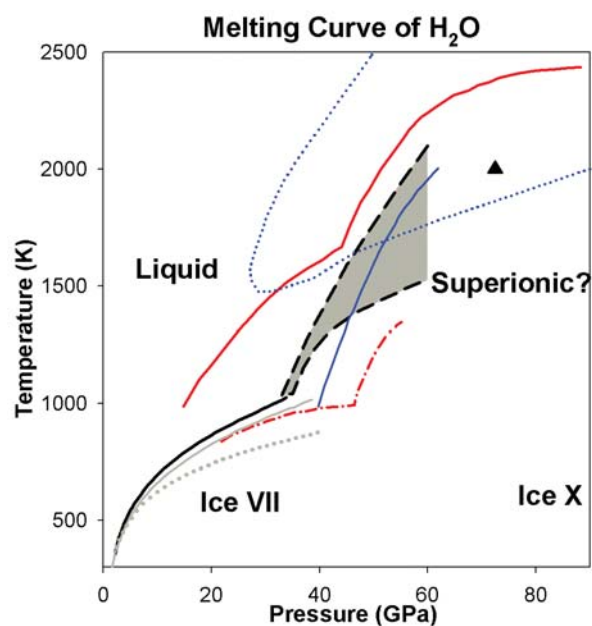


Plate 1. Melting curve of H_2O at high P - T . Black solid line, melting curve of ice VII determined by Raman spectra, optical observation, and X-ray diffraction [Lin *et al.*, 2004a; 2005]; black dashed line and grey area: upper bound and lower bound of the extrapolated melting curve [Lin *et al.*, 2005; also see Fig. 1]; blue dotted line: occurrence of the theoretically predicted superionic phase [Cavazzoni *et al.*, 1999]; red dash line with dots: melting curve determined by Raman spectroscopy in a LHDAC [Goncharov *et al.*, 2005]; blue solid line: theoretically calculated freezing of H_2O [Goncharov *et al.*, 2005]; solid gray line: melting curve determined by angle-dispersive X-ray diffraction [Dubrovinskaia and Dubrovinsky, 2003a,b]; gray dotted line: melting curve determined by energy-dispersive X-ray diffraction in an EHDAC [Frank *et al.*, 2004]; red solid line: optical observation in a LHDAC [Schwager *et al.*, 2004]; solid triangle: liquid to superionic transition in *ab initio* MD calculations [Goldman *et al.*, 2005]. The melting line of Datchi *et al.* [2000] is in agreement with that of Lin *et al.* [2004a, 2005].

THERMODYNAMIC PROPERTIES OF LIQUID AND SOLID H₂O PHASES

A detailed understanding of the EOS properties of liquid and solid phases of H₂O under extreme conditions is essential to the development of accurate models of planetary interiors. Information on the thermodynamic properties of H₂O under extreme conditions has come from a variety of sources, depending on the specific P - T of interest. For the liquid phase under moderate P - T conditions, a large amount of experimental data has been combined into EOS models based on highly parameterized formulations of the Helmholtz free energy [Wagner *et al.*, 2002]. Although this has proven to be quite useful for interpolation of data, the highest P - T conditions that are relevant to planetary science fall outside the range of these models, so their direct use would require large extrapolations with questionable levels of accuracy. For this reason, EOS models for liquid water under extreme P - T conditions have been based on either shock wave experiments [Walsh *et al.*, 1957] or MD simulations [Belonoshko *et al.*, 1991; Brodholt *et al.*, 1993; Sakane *et al.*, 2001]. In particular, the TIP4P empirical potential [Jorgensen *et al.*, 1983] has been used to tabulate P - V - T data for water up to 2500 K and 35 GPa. By adding virial terms to a modified Redlich Kwong-style EOS equation:

$$P = \frac{RT}{V-b} - \frac{a}{T^{1/2}V(V+b)} + \frac{c}{V} + \frac{d}{V^2} + \frac{e}{V^3} + \frac{f}{V^4}$$

$$a = -582468 - 3038.79T - 9.24574 \times 10^{-3}T^2 + 3.02674 \times 10^9/T^2$$

$$b = -3.90463 \times 10^{-2} - 0.991078V$$

$$c = 3.64905 \times 10^4$$

$$d = -1.02451 \times 10^7$$

$$e = -1.79681 \times 10^8$$

$$f = 2.18437 \times 10^9$$

where V is the volume in cm³/mol, P is in bars and T is in Kelvin, the simulation data can be faithfully reproduced over a wide range of phase-space [Brodholt *et al.*, 1993]. However, some care should be exercised when using empirical potentials like TIP4P for describing water under high- P conditions. As mentioned earlier, simple empirical models typically do not allow for intramolecular dissociation reactions, which most certainly readily occur in liquid water for pressures above 15 GPa [Holzapfel, 1969].

Most thermodynamic data on ice under pressure have come from room temperature DAC measurements due to the difficulty of simultaneously achieving high P - T in a DAC and the rapid rise in T characteristic of shock experiments. As shown in Table 1, DAC experiments on ice VII have been reported and used to fit different isothermal models with relatively good levels of agreement for properties such as the bulk modulus

and the equilibrium volume. However, in the development of a complete EOS model for ice VII, some difficulties are encountered due to the fact that ice VII is not recoverable under ambient P - T conditions, which could otherwise provide a convenient reference point for determining the Gibbs free energy. To deal with this complication, EOS models for ice VII are usually developed by taking advantage of the fact that along the melting curve, the Gibbs free energy of the liquid and the solid are equal. By starting from an appropriate EOS for the liquid phase (*e.g.* from shock wave measurements or MD simulations) and matching to an accurate measurement of the melting curve, thermodynamically consistent EOS models for both liquid and solid H₂O can be readily constructed [Frank *et al.*, 2004; Dolan *et al.*, 2005].

PLANETARY AND GEOPHYSICAL APPLICATIONS

The discontinuous and rapid increase in the melting curve of H₂O at and above the triple point at ~35 to 47 GPa indicates a large increase in $\Delta V/\Delta S$ (entropy versus volume change), significant changes in the physical properties of H₂O, and possible existence of a solid ice phase at higher P - T . The unusual behavior of H₂O has several important implications to understanding planetary interiors, including Earth's. Based on extrapolations of the H₂O melting curve [Datchi *et al.*, 2000], Bina and Navrotsky [2000] suggested that ice VII exists in portions of the coldest subducting slabs after H₂O is liberated from hydrous minerals by successive dehydration processes. Although recent studies on the melting curve of H₂O are consistent with the calculations, an eutectic behavior and melting point depression of H₂O with surrounding materials are expected in a multi-component system such as the Earth's mantle, making the presence of solid ice VII phase in the Earth's mantle unlikely. Depending on the curvature of the extrapolated melting curve above the triple point, the solid-liquid phase boundary may intersect the isentropes of Neptune and Uranus and the geotherm of Earth's lower mantle (*i.e.*, at 60 GPa based on the extrapolated melting curve by Lin *et al.* [2005]) (Figures 1, Plate 1). Thus, H₂O could exist in a solid form at P - T conditions between the middle to lowermost mantle and the intermediate layers of Neptune and Uranus. Based on seismic and geodynamic data, a high viscosity layer with strongly suppressed flow-induced deformation and convective mixing has been proposed to exist near 2000 km depth [Forte and Mitrovica, 2001]. The intersection between the melting curve of H₂O and the mantle geotherm at approximately 60 GPa suggests significant changes in the physical properties of H₂O and the stability of hydrous minerals within the mid-lower mantle and may provide an additional explanation for its viscosity heterogeneity [Forte and Mitrovica, 2001; Lin *et al.*, 2005]. However, if the significant increase in the melting curve

Table 1. Comparison of reported EOS parameters determined for ice VII and liquid water by isothermal compression at 300 K. The transition to ice X (~40–60 GPa) is often neglected in determining the EOS parameters of ice VII. V_0 : the zero pressure volume; K_{0T} : isothermal bulk modulus at ambient conditions; K'_{0T} : the derivative of the isothermal bulk modulus at ambient conditions; P: the pressure range that the measurements were taken over; EOS: 3rd order Birch-Munaghan (BM), Vinet, or Murnaghan (M).

	V_0 (cm ³ /mol)	K_{0T} (GPa)	K'_{0T}	P (GPa)	EOS	Authors
Ice VII:						
	12.3	23.7	4.15	4.3–128	BM	Hemley <i>et al.</i> , 1987
	14.52	4.26	7.75	2.2–170	Vinet	Loubeyre <i>et al.</i> , 1999
	12.3	23.9	4.2	3.16–18.55	BM	Fei <i>et al.</i> , 1993
	12.22	25.04	3.66	3.16–128	M	Dolan <i>et al.</i> , 2005
	12.4	21.1	4.4	6.82–60.52	BM	Frank <i>et al.</i> , 2004
Liquid:						
	18.07	2.21	6.029	0.05–0.8	M	Dolan <i>et al.</i> , 2005

is due to the occurrence of a superionic phase [Cavazzoni *et al.*, 1999; Goncharov *et al.*, 2005; Goldman *et al.*, 2005], fast protonic diffusion could enhance chemical reactivity with silicates and oxides and lead to the formation of hydrous silicate and oxide compounds in the Earth's lower mantle. Based on cosmochemical abundances and density profiles of Uranus and Neptune, H₂O, CH₄, and NH₃ are presumed to be major components in the middle layers of these icy planets. Fully disassociated, ionic H₂O and NH₃ (and possible CH₄) would lead to reactions between these components, and the formation of complex oxygen, nitrogen, carbon, and hydrogen compounds. In addition, the reaction of H₂O with iron at high P-T to form iron hydrides (FeH_x) provides a mechanism for the incorporation of hydrogen as a light element into growing Earth's core [Okuchi, 1997; Williams and Hemley, 2001; Ohtani *et al.*, 2005], but also raises complications regarding possible solid ice phase in the Earth's mantle.

Knowledge of the EOS of liquid H₂O is also needed to understand the behavior of possible hydrous fluids and melts that may be present in the Earth's mantle. In addition to the formation of fluids/melts upon dehydration of hydrous minerals in the subducting slabs, regions deeper in the mantle that may become saturated in H₂O would result in formation of dense melts rich in H₂O, MgO, SiO₂, and other components that fractionate into the melt. Since H₂O is likely the most compressible component in the melt, the presence and concentration of H₂O would have a large influence on the melt density and physical properties at depth [*e.g.* Richet and Polian, 1998; Matsukage *et al.*, 2006]. High-pressure studies have shown that wadsleyite and ringwoodite, two major minerals in the transition zone (410–660 km depth), have anomalously high water solubility on the order of 1 wt% (and as much as 3 wt%) whereas the solubility of water in upper- and lower-mantle minerals is 5 to 10 times lower [*e.g.* Hohlstedt

et al., 1996; Bolfan-Casanova *et al.*, 2000; Murakami *et al.*, 2002]. Bercovici and Karato [2003] proposed that a thin melt layer may form at 41-km depth if the wadsleyite in the transition zone contained more hydrogen than is soluble into olivine just above 410-km. Thus, passively upwelling mantle crossing the 410-km discontinuity would experience dehydration-induced partial melting. In order to test this hypothesis, it is necessary to know if such a melt layer at 410-km depth would be denser than the solid material above it. Therefore, the physical properties of water and hydrous melts and fluids must be further understood for geodynamic modeling of Earth's potential deep-water cycle.

Acknowledgments. This work was performed under the auspices of the U.S. Department of Energy at the University of California/Lawrence Livermore National Laboratory under Contract No. W-7405-Eng-48. Support for the study was also provided by the Lawrence Livermore Fellowship to J. F. Lin. We thank S. D. Jacobsen for numerous comments and discussions. We also thank G. Galli, W. J. Evans, Z. Jenei, E. Gregoryanz, M. Somayazulu, B. Militzer, V. V. Struzhkin, S. Gramsch, R. J. Hemley, and H. K. Mao for helpful discussions. J. F. Lin and E. Schwegler contributed equally to the paper.

REFERENCES

- Alfe, D (2003), First-principles simulations of direct coexistence of solid and liquid aluminum, *Phys. Rev. B* 68, 064423.
- Angel, R. J., D. J. Frost, N. L. Ross, and R. Hemley (2001), Stabilities and equations of state of dense hydrous magnesium silicates, *Phys. Earth Planet. Int.*, 127, 181–196.
- Aoki, K., H. Yamawaki, M. Sakashita, and H. Fujihisa (1996), Infrared absorption study of the hydrogen-bond symmetrization in ice to 110 GPa, *Phys. Rev. B*, 54, 15673–15677.
- Bassett, W. A., A. H. Shen, M. Bucknum, and I. M. Chou (1993), A new diamond anvil cell for hydrothermal studies to 10 GPa and -190°C to 1100°C, *Rev. Sci. Instrum.*, 64, 2340–2345.

- Bell, D., and G. Rossman (1992), Water in Earth's mantle: The role of nominally anhydrous minerals: *Science*, 255, 1391–1397.
- Benoit, M., M. Bernasconi, P. Focher, and M. Parrinello (1996), New high-pressure phase of ice, *Phys. Rev. Lett.*, 76, 2934–2936.
- Benoit, M., D. Marx, and M. Parrinello (1998), Tunneling and zero-point motion in high-pressure ice, *Nature*, 392, 258–261.
- Bercovici, D., and S. Karato (2003), Whole-mantle convection and the transition-zone water filter, *Nature*, 425, 39–44.
- Bernasconi, M., P. L. Silvestrelli, and M. Parrinello (1998), *Ab initio* infrared absorption study of the hydrogen-bond symmetrization in ice, *Phys. Rev. Lett.*, 81, 1235–1238.
- Bina, C. R., and A. Navrotsky (2000), Possible presence of high-pressure ice in cold subducting slabs, *Nature*, 408, 844–847.
- Bolfan-Casanova, N., H. Keppler, and D. Rubie (2000), Water partitioning between nominally anhydrous minerals in the MgO–SiO₂–H₂O system up to 24 GPa: implications for the distribution of water in the earth's mantle, *Earth Planet. Sci. Lett.*, 182, 209–221.
- Brodholt, J., and B. Wood (1993), Simulations of the structure and thermodynamic properties of water at high pressures and temperatures, *J. Geophys. Res.*, 98, 519–536.
- Brown, J. M., and T. J. Shankland (1981), Thermodynamic parameters in the Earth as determined from seismic profiles, *Geophys. J. R. Astr. Soc.*, 66, 579–596.
- Cavazzoni, C., *et al.* (1999), Behavior of ammonia and water at high pressure and temperature: implications for planetary physics, *Science*, 283, 44–46.
- Celliers, P. M., *et al.* (2004), Electronic conduction in shock-compressed water, *Phys. Plasmas*, 11, L41–L44.
- Chau, R., A. C. Mitchell, R. W. Minich, and W. J. Nellis (2001), Electrical conductivity of water compressed dynamically to pressures of 70–180 GPa (0.7–1.8 Mbar), *J. Chem. Phys.*, 114, 1361–1365.
- David, H. G., and S. D. Hamann (1959) The chemical effects of pressure. Part 5. The electrical conductivity of water at high shock pressures, *Trans. Faraday Soc.*, 55, 72–78.
- Datchi, F., P. Loubeyre, and R. LeToullec (2000), Extended and accurate determination of the melting curves of argon, helium, ice (H₂O), and hydrogen (H₂), *Phys. Rev. B*, 61, 6535–6546.
- Demontis, P., R. LeSar, and M. L. Klein (1988), New high-pressure phases of ice, *Phys. Rev. Lett.*, 60, 2284–2287.
- de Pater, I., and J. J. Lissauer (2001), *Planetary Sciences*, pp. 544, University Cambridge Press.
- Dolan, D. H., J. N. Johnson, and Y. M. Gupta (2005), Nanosecond freezing of water under multiple shock wave compression: Continuum modeling and wave profile measurements *J. Chem. Phys.*, 123, 064702.
- Dubrovinskaia, N., and L. Dubrovinsky (2003a), Melting curve of water studied in externally heated diamond-anvil cell, *High Pressure Res.*, 23, 307–310.
- Dubrovinskaia, N., and L. Dubrovinsky (2003b), Whole-cell heater for the diamond anvil cell, *Rev. Sci. Instrum.*, 74, 3433–3437.
- Fei, Y., H. K. Mao, and R. J. Hemley (1993), Thermal expansivity, bulk modulus, and melting curve of H₂O-ice VII to 20 GPa, *J. Chem. Phys.*, 99, 5369–5373.
- Forte, A. M., and J. X. Mitrovica (2001), Deep-mantle high-viscosity flow and thermochemical structure inferred from seismic and geodynamic data, *Nature*, 410, 1049–1056.
- Frank, M.R., Y. Fei, and J. Hu (2004), Constraining the equation of state of fluid H₂O to 80 GPa using the melting curve, bulk modulus, and thermal expansivity of Ice VII, *Geochim. Cosmochim. Acta*, 68, 2781–2790.
- Frost, D. J., *et al.* (2004), Experimental evidence for the existence of iron-rich metal in the Earth's lower mantle, *Nature*, 428, 409–412.
- Goldman, N., L. E. Fried, I.-F. W. Kuo, and C. J. Mundy (2005), Bonding in the superionic phase of water, *Phys. Rev. Lett.*, 94, 217801.
- Goncharov, A. F., V. V. Struzhkin, M. Somayazulu, R. J. Hemley, and H. K. Mao (1996), Compression of H₂O ice to 210 GPa: evidence for a symmetric hydrogen-bonded phase, *Science*, 273, 218–220.
- Goncharov, A. F., V. V. Struzhkin, H. K. Mao, and R. J. Hemley (1999), Raman spectroscopy of dense ice and the transition to symmetric hydrogen bonds, *Phys. Rev. Lett.*, 83, 1998–2001.
- Goncharov, A. F., *et al.* (2005), Dynamic ionization of water under extreme conditions, *Phys. Rev. Lett.*, 94, 125508.
- Hamann, S. D., and M. Linton (1969), Electrical conductivities of aqueous solutions of KCl, KOH and HCl, and the ionization of water a high shock pressures, *Trans. Faraday Soc.*, 65, 2186–2196.
- Hansen, C. J., L. Esposito, A. I. F. Stewart, J. Colwell, A. Hendrix, W. Pryor, D. Shemansky, and R. West. (2006) Enceladus' water vapor plume. *Science*, 311, 1422–1425.
- Hemley, R. J., *et al.* (1987), Static compression of H₂O-ice to 128 GPa (1.28 Mbar). *Nature*, 330, 737–740.
- Holmes, N. C., W. J. Nellis, W. B. Graham, and G. E. Walrafen (1985), Spontaneous Raman scattering from shocked water, *Phys. Rev. Lett.*, 55, 2433–2436.
- Holzappel, W. B. (1969), Effect of pressure and temperature on the conductivity and ionic dissociation of water up to 100 kbar and 1000°C, *J. Chem. Phys.*, 50, 4424–4428.
- Holzappel, W. B. (1972), On the symmetry of hydrogen bonds in ice VII, *J. Chem. Phys.*, 56, 712–715.
- Hubbard, W. B., *et al.* (1991), Interior structure of Neptune: comparison with Uranus, *Science*, 253, 648–651.
- Jorgensen, W. A., J. Chandrasekhar, J. D. Madura, R. W. Impley, and M. L. Klein, Comparison of simple potential functions for simulating liquid water, *J. Chem. Phys.*, 79, 926–935.
- Katoh, E., H. Yamawaki, H. Fujihisa, M. Sakashita, and K. Aoki (2002), Protonic diffusion in high-pressure ice VII, *Science*, 295, 1264–1266.
- Kawamoto, T., S. Ochiai, and H. Kagi (2004), Changes in the structure of water deduced from the pressure dependence of the Raman OH frequency, *J. Chem. Phys.*, 120, 5867–5870.
- Kohlstedt, D., H. Keppler, and D. Rubie (1996), Solubility of water in the α , β and γ phases of (Mg, Fe)₂SiO₄, *Contrib. Mineral. Petrol.*, 123, 345–357.
- Komabayashi, T. (2006), Phase relations of hydrous peridotite: implications for water circulation in the Earth's mantle, *this volume*.

- Lin, J. F., *et al.* (2004a), High pressure-temperature Raman measurements of H₂O melting to 22 GPa and 900 K, *J. Chem. Phys.*, 121, 8423–8427.
- Lin, J. F., M. Santoro, V. V. Struzhkin, H. K. Mao, and R. J. Hemley (2004b), *In situ* high pressure-temperature Raman spectroscopy technique with laser-heated diamond anvil cells, *Rev. Sci. Instrum.*, 75, 3302–3306.
- Lin, J. F., *et al.* (2005), Melting behavior of H₂O at high pressures and temperatures, *Geophys. Res. Lett.*, 32, L11306, doi:10.1029/2005GL022499.
- Loubeyre, P., R. LeToullec, E. Wolanin, M. Hanfland, and D. Hausermann (1999), Modulated phases and proton centering in ice observed by X-ray diffraction up to 170 GPa, *Nature*, 397, 503–506.
- Mahoney, M. W., and W. L. Jorgensen (2000), A five-site model for liquid water and the reproduction of the density anomaly by rigid, nonpolarizable potential functions, *J. Chem. Phys.*, 112, 8910–8922.
- Matsukage, K. N., Z. Jing, and S.-i. Karato (2006) Density of hydrous silicate melt at the conditions of Earth's deep upper mantle. *Nature*, 438, 488–491.
- Mitchell, A. C., and W. J. Nellis (1982), Equation of state and electrical conductivity of water and ammonia shocked to the 100 GPa (1 Mbar) pressure range, *J. Chem. Phys.* 76, 6273–6281.
- Murakami, M., K. Hirose, H. Yurimoto, S. Nakashima, and N. Takafuji (2002), Water in earth's lower mantle, *Science*, 295, 1885–1887.
- Nellis, W. J., *et al.* (1988), The nature of the interior of Uranus based on studies of planetary ices at high dynamic pressure, *Science*, 240, 779–781.
- Ogitsu, T., E. Schwegler, F. Gygi, and G. Galli (2003), Melting of lithium hydride under pressure, *Phys. Rev. Lett.*, 91, 175502.
- Ohtani, E., N. Hirao, T. Kondo, M. Ito, and T. Kikegawa (2005), Iron-water reaction at high pressure and temperature, and hydrogen transport into the core, *Phys. Chem. Miner.*, 32, 77–82.
- Okuchi, T. (1997) Hydrogen partitioning into molten iron at high pressure: implications for the Earth's core. *Science*, 278, 1781–1784.
- Pauling, L. (1935), Structure and entropy of ice and of other crystals with some randomness of atomic arrangement, *J. Am. Chem. Soc.*, 57, 2680–2684.
- Petrenko, V. F., and R. W. Whitworth (1999), *Physics of ice*, pp. 252–283, Oxford Univ. Press, New York.
- Polian, A., and M. Grimsditch, (1984), New high-pressure phase of H₂O: Ice X, *Phys. Rev. Lett.*, 52, 1312–1314.
- Rahman, A., and F. H. Stillinger (1971), Molecular dynamics study of liquid water, *J. Chem. Phys.*, 33, 3336–3359.
- Richet, P., and A. Polian (1998) Water as a dense icelike component in silicate glass. *Science*, 281, 396–398.
- Sakane, S., W. Liu, D. J. Doren, E. L. Shock, and R. H. Wood (2001), Prediction of the Gibbs energies and an improved equation of state for water at extreme conditions from ab initio energies with classical simulations, *Geochim. Cosmochim. Acta*, 65, 4067.
- Sanz, E., C. Vega, J. L. F. Abascal, and L. G. MacDowell (2004), Phase diagram of water from computer simulation, *Phys. Rev. Lett.*, 92, 255701.
- Schilling, J. G., M. B. Bergeron, and R. Evans (1980), Halogens in the mantle beneath the North Atlantic, *Phil. Trans. R. Soc. London A*, 297, 147–178.
- Schwegler, E., G. Galli, and F. Gygi (2000), Water under pressure, *Phys. Rev. Lett.*, 84, 2429–2432.
- Schwegler, E., G. Galli, F. Gygi, and R. Q. Hood (2001), Dissociation of water under pressure, *Phys. Rev. Lett.*, 87, 265501.
- Schwager, B., L. Chudinovskikh, A. Gavriluk, and R. Boehler (2004), Melting curve of H₂O to 90 GPa measured in a laser-heated diamond cell, *J. Phys. Condens. Matter*, 16, S1177–S1179.
- Smyth, J. R. (1987), β -Mg₂SiO₄: a potential host for water in the mantle? *Am. Mineral.*, 72, 1051–1055.
- Smyth, J.R. and S.D. Jacobsen (2006), Nominally anhydrous minerals and Earth's deep water cycle, *this volume*.
- Strässle, Th., A. M. Saitta, Y. Le Godec, G. Hamel, S. Klotz, J. S. Loveday, and R. J. Nelmes (2006), Structure of dense liquid water by neutron scattering to 6.5 GPa / 670 K, *Phys. Rev. Lett.*, 96, 1067801.
- Williams, Q., and R. J. Hemley (2001), Hydrogen in the deep earth, *Annu. Rev. Earth Planet. Sci.*, 29, 365–418.
- Wagner, W., and A. Pruß (2002), The IAPWS formulation 1995 for the thermodynamic properties of ordinary water substance for general and scientific use, *J. Phys. Chem. Ref. Data*, 31, 387–535.
- Walsh, J. M., and M. H. Rice (1957), Dynamic compression of liquids from measurements on strong shock waves, *J. Chem. Phys.*, 26, 815–823.

